



# A probabilistic seismic hazard analysis in SE Iran; case study: Kerman province

Mehrdad Balouch<sup>1</sup> · Majid Nemati<sup>2,3</sup> · Mohammad Hossein Bagheripour<sup>1</sup> · Ahmad Rashidi<sup>3</sup>

Received: 25 May 2022 / Accepted: 2 October 2023 / Published online: 21 November 2023  
© The Author(s), under exclusive licence to Universidad Complutense de Madrid 2023

## Abstract

Kerman province in SE Iran has always experienced devastating earthquakes. Therefore, it is necessary to carry out an up-to-date probabilistic seismic hazard analysis (PSHA) in order to the risk reduce and increase the resilience of the infrastructures. This study provides PSHA with emphasis on uncertainties in different steps of analysis. To create an integrated seismic catalog with moment magnitude, a magnitude conversion algorithm was proposed which can be applied with the reference to IRSC main catalog. To achieve the best results, active seismic zones of Kerman province and its around areas, have been carefully identified. Seismic source zones were modeled by four criteria: seismicity, faults, geological conditions, and focal mechanisms. Seismicity parameters (Gutenberg-Richter recurrence law coefficients,  $M_{\max}$  and  $M_{\min}$ , as well as activity rate) were determined for all the seismic source zones. Ground-motion models have been applied in accordance with the region and the existing uncertainties have been identified and reduced as much as possible. The results of this study are presented in form of bedrock seismic hazard maps for PGA and spectral acceleration in 0.2 s and 1.0 s periods with a probability of 2% and 10% in 50 years, to meet all structural design needs in the region. Our results indicate the maximum and minimum PGA with the 475-year return period (0.58 g and 0.05g) are related to the Faryab city, and the Lut plain, respectively. Also, our results of the 2475- return period show Faryab city and Lut plain have highest and lowest PGA (0.92 g and 0.1 g), respectively.

**Keywords** Probabilistic Seismic Hazard Analysis (PSHA) · Seismic hazard maps · Peak Ground Acceleration (PGA) · Seismic design · Kerman province · Iran

## Resumen

Históricamente, la provincia de Kerman, SE Irán, ha experimentado muchos terremotos devastadores. Es por tanto necesario hacer una puesta al día mediante un análisis probabilístico de peligros sísmicos (PSHA) con la idea de reducir los riesgos y aumentar la resiliencia de las infraestructuras. El estudio de PSHA presentado está desarrollado en diferentes etapas. Para crear un catálogo integrado de sismos con momento de magnitud, se ha propuesto un algoritmo de conversión de magnitudes que puede ser aplicado con un catálogo base de IRSC. Para obtener los mejores resultados se han identificado las zonas sísmicas de la provincia de Kerman y de zonas próximas. Las zonas de origen sísmico fueron diferenciadas bajo cuatro criterios: sismicidad, fallas, condiciones geológicas y mecanismos focales. Los parámetros sísmicos (Ley de recurrencia Gutenberg-Richter,  $M_{\max}$  y  $M_{\min}$ , y el grado de actividad) fueron determinados para todas las zonas de origen de los sismos. Los modelos de movimientos profundos han sido aplicados de acuerdo con cada región. Pudiéndose detectar incertidumbres y reducirlas todo lo posible. Los resultados de este estudio son presentados en forma de mapas de peligros sísmicos para PGA, y aceleración espectral de periodos de 0,2 a 1.0 s con una probabilidad del 2% al 10% en 50 años, para encontrar el

✉ Majid Nemati  
nemati\_majid\_1974@uk.ac.ir

<sup>1</sup> Department of Engineering, Faculty of Civil Engineering of Shahid, Bahonar University of Kerman, Kerman, Iran

<sup>2</sup> Department of Geology, Faculty of Science of Shahid, Bahonar University of Kerman, Kerman, Iran

<sup>3</sup> Department of Earthquake Research, Shahid Bahonar University of Kerman, Kerman, Iran

diseño estructural necesario en la región. Nuestros resultados abarcan el máximo y mínimo PGA con un periodo de retorno de 475 años (0,58 g y 0,1 g) para la ciudad de Faryad y la llanura Lt respectivamente. Por otro lado, nuestros resultados con periodo de retorno de 2.475 muestra que la ciudad de Faruad y la llanura de Lut tienen los valores más altos y más bajos de PGA (0,92 g y 0,1 g) respectivamente.

**Palabras clave** Análisis probabilístico de riesgos sísmicos (PSHA) · Mapa de peligros sísmicos · Pico de aceleración profundo (PGA) · Diseño sísmico · Provincia Kerman · Irán

## 1 Introduction

Kerman province ( $26^{\circ}$ – $32^{\circ}$  N,  $54^{\circ}$ – $60^{\circ}$  E) is one of the most seismically active regions in Iran, which is located within the Iranian plate, and convergence zone of Eurasian and Arabian continental plates (Fig. 1). Also, the province is located in the vicinity of Makran subduction zone where the Oman oceanic crust is subducting under the Makran continental crust. According to the historical and instrumental records, since 1854, one ( $M_w \geq 7.0$ ) and more than 17 ( $6.0 \leq M_w < 7.0$ ) instrumental events and 5 ( $5.5 \leq M_s < 6.5$ ) historical and pre instrumental earthquakes

(Mirzaei et al., 1997; Nemati & Derakhshani, 2021; Kamali et al. 2023; Nemati et al., 2020) have occurred in this region. The high seismicity rate of Kerman province has been caused high casualties and severe destruction of human and buildings over the last decades (e.g. Rashidi et al., 2019, 2021). The first significant event recorded in the historical catalog of this area is related to 1864 Chatrud earthquake ( $M_w \sim 6.1$ ), which due to its proximity to the Kerman city led to the significant human casualties and severe destruction in Kerman city (Ambraseys & Melville, 1982). The 1911 Ravar ( $M_w 6.2$ ), 1923 Lalehzar ( $M_w 6.7$ ), and 1977 Zarand ( $M_w 5.9$ ) earthquakes (Ambraseys &

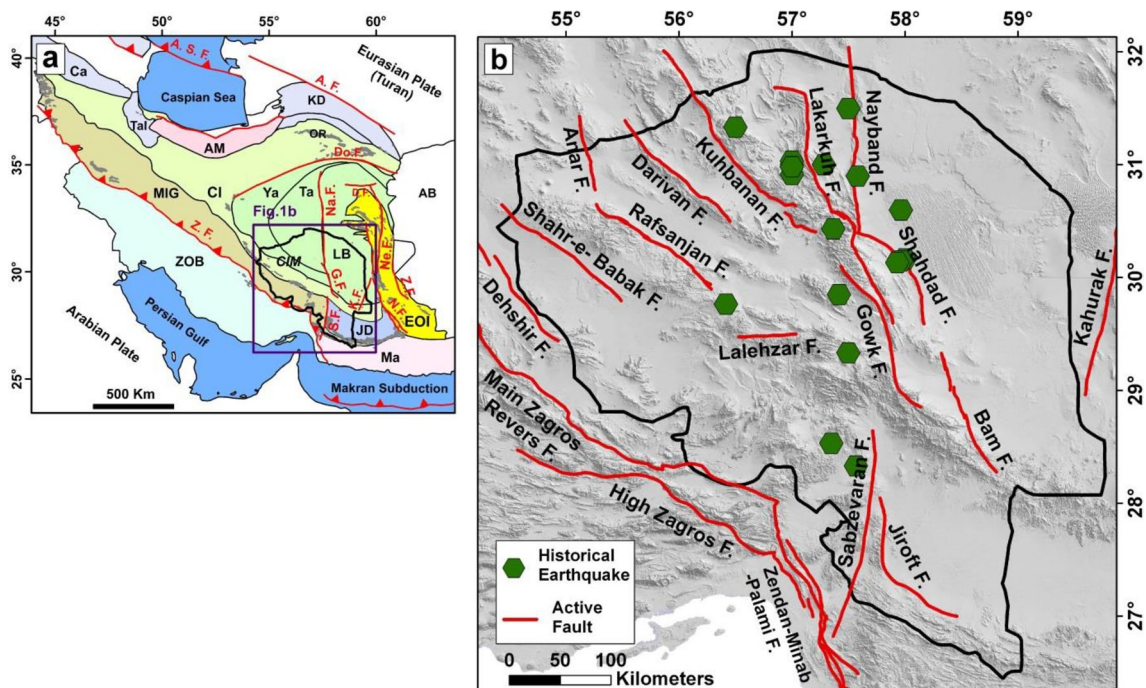


**Fig. 1** Tectonic setting of the study area. **a** The regional structures of the Arabia- Eurasia convergence and the position of the Kerman province. *EOI* Eastern Iran orogen, *Ca* Caucasus, *KD* Kopet Dagh, *AM* Alborz Mountains, *Tal* Talesh, *MIG* zone of metamorphic rocks and intruded granitoides, *CIM* Central Iranian Microcontinent, *Ta* Tabas, *Ya* Yazd, *CI* Central Iran, *AB* Afghan block, *LB* Lut block,

*ZOB* Zagros orogenic belt, *Ma* Makran, *JD* Jazmurian depression, *OR* ophiolitic rocks, *Ne.F* Nehbandan fault, *N.F* Nosratabad fault, *K.F.* Kahourak fault, *Z.F.* Zahedan fault, *D.F.* Dashte Bayaz fault, *Do. F* Doruneh fault, *S.F.* Sabzevaran fault, *G.F.* Gowk fault, *Na.F.* Nayband fault, *A.F.* Ashkabad fault, *A.S.F.* Apsheron Sill fault. **b** Active faults map with historical earthquake in the area (See references in Table 1)

**Table 1** Most significant earthquakes of Kerman province from 1800 to 2020

Date	Region	Causative fault		Mag. ( $M_w$ )	Mag. ( $M_w$ )
		Name	References		
1864-01-17	Chatroud	Chatroud F.	Adapted from Berberian (2014)	6.1	Many killed, Severe destruction of Kerman city
1875-05-01	Kouhbanan	Kouhbanan F.	Adapted from Berberian (2014)	6.1	No casualties
1897-05-27	Chatroud	Chatroud F.	Adapted from Berberian (2014)	5.7	Several killed, Damage to the city of Kerman
1911-04-18	Ravar	Lakarkouh F.	Adapted from Berberian (2014)	6.2	700 killed, complete destruction of Ravar city
1923-09-22	Lalehzar	Lalehzar F.	Adapted from Berberian (2014)	6.7	More than 200 people were killed
1947-10-03	Ghal-e-Ganj	Jiroft F.	Adapted from Berberian (2014)	6.1	Unknown
1948-07-05	Golbaf	Golbaf-Sirch F.	Adapted from Berberian (2014)	6.1	Unknown
1977-12-19	Zarand	Kouhbanan F.	Adapted from Berberian (2014)	5.9	665 killed, 260 injured
1981-06-11	Golbaf	Golbaf-Sirch F.	Berberian et al. (1984)	6.6	1071 killed, 4000 injured (1981-07-28 Golbaf earthquake foreshock)
1981-07-28	Sirch	Golbaf-Sirch F.	Berberian et al. (1984)	7.2	1300 killed, 915 injured, 25,000 homeless
1989-11-20	Golbaf	Golbaf-Sirch F.	Berberian and Qorashi (1994)	5.9	40 killed, 45 injured
1998-03-14	Shahdad	Golbaf-Sirch F.	Walker et al. (2001)	6.6	5 killed, 50 injured
1999-03-04	Faryab	Faryab Shear Zone	Rashidi et al. (2020)	6.6	Unknown
2003-12-26	Bam	Bam F.	Fielding et al. (2005)	6.6	More than 26,000 killed, 30,000 injured, tens of thousands homeless, complete destruction of Bam city
2005-02-22	Zarand	Kouhbanan F.	Talebian et al. (2006a, 2006b)	6.4	612 killed, 1411 injured
2010-12-20	Rigan	Kanurak F.	Walker et al. (2013)	6.5	11 killed, 100 injured
2017-12-01	Hojedk	Lakarkouh F.	Nemati et al. (2020)	6.1	No casualties

Melville, 1982), caused ~ 700, ~ 200, and ~ 665 casualties respectively, and imposed significant damages to nearby cities. The 1981 Golbaf earthquakes ( $M_w$  6.6 and  $M_w$  7.2) (Berberian et al., 2001) occurred within one month, causing death and injuring of ~ 7000 people and left more than ~ 25,000 homeless people. In 2003, the Bam earthquake ( $M_w$  6.6) was one of the most catastrophic of urban events in Iran and the Kerman region. According to official reports, its human casualties was ~ 26,000 people, and extremely destroyed the Bam city. The latest significant casualties from an earthquake in the region is related to the 2005 Zarand earthquake ( $M_w$  6.4) (Nemati & Gheitanchi, 2011; Talebian et al., 2006a, 2006b), which included more than ~ 600 human casualties. The 2010 Rigan ( $M_w$  6.5) (Nemati & Tatar, 2015; Walker et al., 2013) and 2017 Hojedk ( $M_w$  6.1) (Savidge et al., 2019) earthquakes are the last significant earthquakes in the region, which didn't cause significant economic and human losses. As is clear, Kerman province in SE Iran has always suffered from devastating earthquakes (Table 1). Therefore, it is necessary to carry out an up-to-date probabilistic seismic hazard analysis to reduce the risk and increase the resilience of the infrastructures. In this study, an integrated catalog containing 13,000 instrumental and historical earthquakes from 1800 to 2020 was compiled to perform the analysis. The seismogenic zones in Kerman province were defined. Seismicity parameters (Gutenberg-Richter recurrence law

coefficients,  $M_{max}$  and  $M_{min}$ , as well as activity rate) for all the seismic source zones were determined. A hybrid ground-motion predictive model, which was developed based on those sources, was appropriate for the region. Finally, seismic hazard maps for bedrock, which are one of the basic design requirements, were presented for Pick Ground Acceleration (PGA).

During the recent years some seismic hazard maps for the Iran was obtained by some researcher. One of the first seismic hazard maps of Iran has presented by Tavakoli and Ghafory-Ashtiany (1999) using 20 seismic source zones in terms of Peak Ground Acceleration (PGA) with a 10% probability of exceedance in 50 years. Moinfar et al. (2012) evaluated PGA for Iran using PSHA in 475 years return period. Their map has been developed for the Housing and Building Research Center of Iran (BHRC) for use in the Iranian Seismic Code (Standard No 2800, 4th edition). Yazdani and Kowsari (2013a, 2013b) using the Bayesian theory, Mohammadi and Bayrak (2016) using the Gumbel's third asymptotic distribution (GIII), and Mahsuli et al. (2019) using reliability methods, have presented seismic hazard maps for Iran. However, due to the development of these maps at the national level and their lack of high-precision and small-scale seismic source zones, the results appear to be accurate. In addition to these studies, other probabilistic analysis have been performed at a national level (Salahshoor et al., 2018; Taherian & Kalantari, 2019; Talebi et al.,

2017). However, despite the high seismicity rate of the Kerman region, only two probabilistic seismic hazard analysis have been performed, which is limited to the parts of this province (Dehghan-Manshadi et al., 2020; Saafizaadeh & Bagheripour, 2019). Saafizaadeh and Bagheripour (2019) identified a total of 13 seismic source zones around the Kerman city and the results have been presented as PGA for the return periods of 50, 75, and 475 years. A maximum PGA of 0.65 g with a 10% probability of exceedance in 50 years has been proposed for the eastern part of Kerman city (Saafizaadeh and Bagheripour., 2019). Dehghan-manshadi et al. (2020) provided a PGA map and also spectral acceleration diagrams with a 10% probability of exceedance in 50 years for the Kerman, Rafsanjan, and Ravar cities using both time-dependent and time-independent approaches. In this study, the maximum PGA with a 10% probability of exceedance in 50 years (0.35 g and 0.45 g) has been obtained for the areas around the Kerman city using the time-dependent and time-independent approach, respectively.

## 2 Tectonic setting

Tectonic evolution of Iran is dependent on the Tethys oceanic history (Takin, 1972). The current linkage of the some continental blocks of Gondwanian affinity to Eurasia, like the Central Iran (includes Yazd and Tabas sub zones), Lut and Afghan, has resulted from the opening and closure of the Neo-tethys (Berberian & Berberian, 1981). The Neo-tethys subduction beneath central Iran, sutured the plates of Arabian and Iran, then the convergence of continental plates built the Zagros belt. The Zagros belt (Fig. 1a) includes three NW–SE parallel zones: Sanandaj-Sirjan, Urmieh-Dokhtar and Zagros (e.g. Berberian et al., 1982). Kerman province consists of two structural zones of this belt; Urmieh-Dokhtar and Sanandaj-Sirjan, with Central Iran (Tabas and Yazd), Lut, and Jazmurian (Back arc of Makran subduction) zones.

The Neo-tethys subduction stage which continues to the south is traceable in the offshore Makran (McCall, 1997a). The Zendan-Minab-Palami fault system (ZMP on the Fig. 1a), connects the western Makran to the eastern Zagros (Fig. 1) (McCall & Kidd, 1982). In both domains of the ZMP, the inverted velocity model shows two important layers consists of upper crust (up to ~16km) and middle crust (deeper than ~18km) (Shirzad et al., 2019). The upper crust includes two layers: basement and sedimentary with thicknesses of ~10 and ~6 km, respectively. The important active faults cause variations in these layers. The difference between the average velocity of the middle crust in the collision and subduction zones is ~0.5 km/s (Shirzad et al., 2019). However, based on the some studies (e.g. Jackson & McKenzie, 1988), for eastern and southeastern Iran, the thickness of seismogenic zone was considered to be ~15 km.

The variations of the Moho discontinuity beneath Iran by a detailed P receiver function studies was investigated by some researcher (e.g. Taghizadeh-Farahmand et al., 2015). The results of Taghizadeh-Farahmand et al. (2014) about the teleseismic events recorded from 1995 to 2011 at 77 national permanent stations (24 broadband and 53 short period stations) has shown main variations in the crustal thickness, which are dependent on the different geological structures. Generally, the average thickness of crustal beneath Iran suggested about 40–45 km. A thinnest crust of  $\sim 33 \pm 2$  km beneath the Makran subduction zone and the thickest crust of  $\sim 66 \pm 2$  km have been locally obtained beneath the Sanandaj-Sirjan Zone (as the suture zone of the between the Arabian-Eurasian collision). A thick crust of  $\sim 54 \pm 2$  km due to the shortening is observed beneath the Alborz mountain ranges (Taghizadeh-Farahmand et al., 2015) where has experienced earthquakes with different depths (Rashidi & Derakhshani, 2022; Rashidi et al., 2023a; Trifonov et al., 2022).

Tectonic activity in the western and eastern domains of the Lut Block (as a rigid block) with a thin crustal structure have been observed along the basement faults (Ezati et al., 2022a, 2022b; Mehrabi et al., 2021; Rashidi et al., 2022). The eastern limit of the Lut block, Nehbandan fault system (Rashidi et al., 2023b), overprints the Sistan suture zone (SSZ). SSZ separated the Lut and Afghan block (Sengor et al., 1988). The western domain of the Lut Block is included the Nayband, Gowk and Sabzevaran (from north to south) in the Kerman province (Fig. 2). Right-lateral slip rates related to the late Pleistocene and Holocene in the western domain of the Lut Block (at longitude  $\sim 57^\circ 45'$  E) increases from north to south. This southward increase, which shows complex structural evolution, is inferred from the slip rates of Nayband,  $1.8 \pm 0.7$  mm/year (Foroutan et al., 2014); Gowk,  $3.8 \pm 0.7$  mm/year (Walker et al., 2010) and Sabzevaran,  $5.7 \pm 1.7$  mm/year (Regard et al., 2006) faults systems.

Major active fault systems in the Kerman province can be grouped according to their strike into N–S (e.g. Nayband, Gowk, Sabzevaran, Anar, Lakarkuh, Bam), NW–SE (e.g. Shahr-e Babak, Rafsanjan, Darivan, Kuhbanan, Shahdad, Jiroft), and E–W (e.g. Lalehzar) directions. These faults had main role in the seismicity of the Kerman province (Fig. 1c). There is an absence of historical earthquakes events, but a significant number of instrumental earthquakes for the study area. The lack of historical events may be due to the proximity to deserts (Ambraseys & Melville, 2005). The destructive and large events with the gaps in the north, along the Nayband fault and also in the south, along the Sabzevaran fault, are noticeable. Anyway, many small to moderate earthquakes were recorded along these faults.

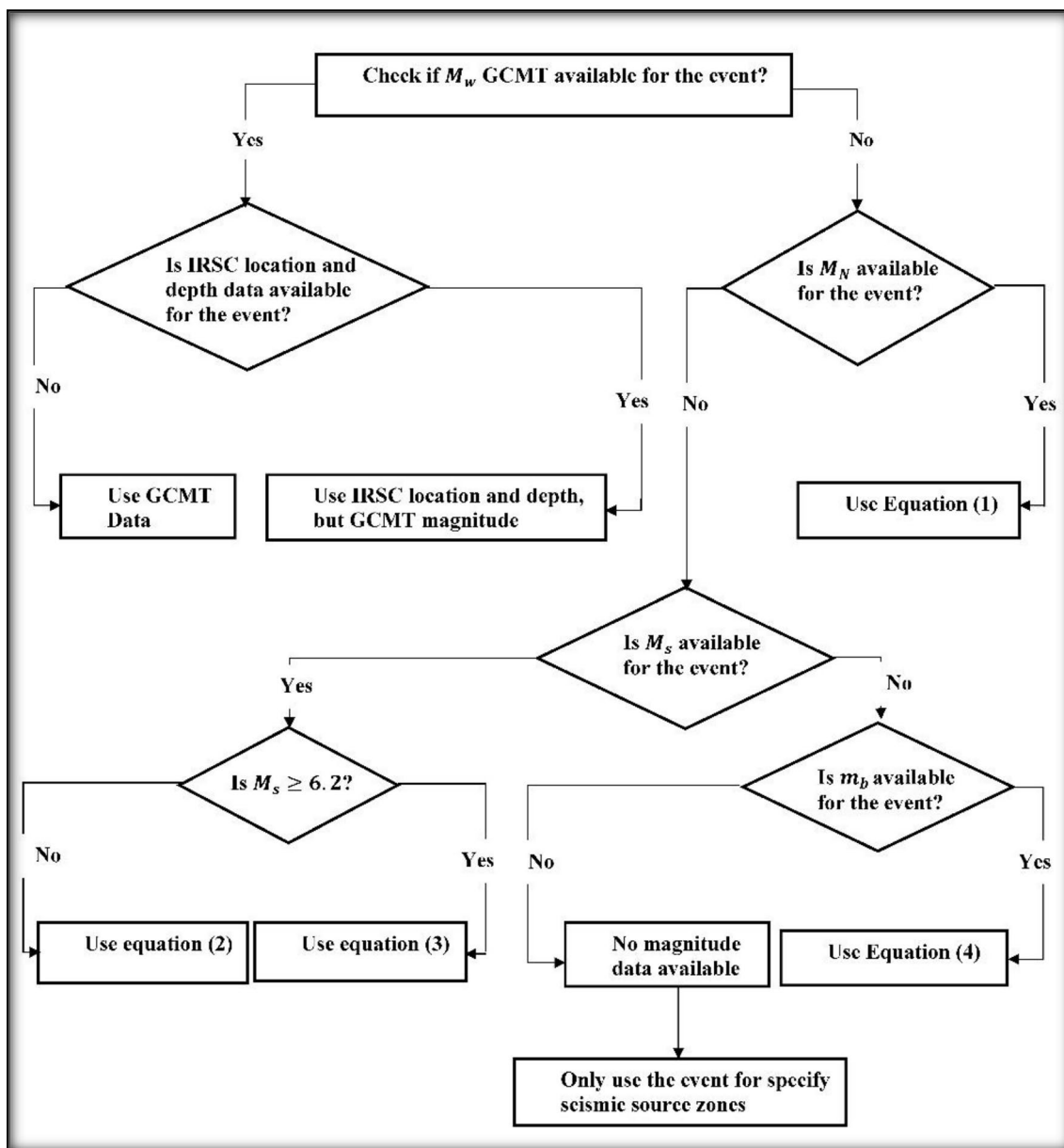


Fig. 2 Proposed algorithm for catalog integration in this study

### 3 Method and data

#### 3.1 Method

The location of future ground shaking due to earthquakes and its intensity are highly uncertain. Using Probabilistic Seismic Hazard Assessment (PSHA), these uncertainties can be quantified and combined to provide a distribution of possible future earthquake shaking. Therefore to investigate the strength of structures to large earthquakes; it is strongly recommended to use the PSHA which generally includes these steps: (1) Identification of seismic sources,

(2) Estimation of seismicity parameters, (3) Selection of GMMs, and (4) Calculation of hazard curves.

Due to the high seismicity rate of Kerman province, especially around the Kerman city with a high population, updating and compiling seismic hazard maps based on PSHA analysis, in order to reduce the risk and increase in the seismic resilience of infrastructures and buildings, is a priority.

In the present study, to more accurate results, active seismic zones of Kerman province and surrounding areas, have been carefully identified. Ground-motion models have been applied in accordance with the region and the

**Table 2** Relationships used to convert different magnitudes to moment magnitude

Mag. type	Mag. Range	Equation	Equation number	References
	$3.5 < M_N < 6.3$	$M_w = 0.739M_N + 1.41$	(1)	Karimiparidari et al (2013)
$M_S$	$3 \leq M_S < 6.2$	$0.67(\pm 0.005)M_S + 2.07(\pm 0.03)$	(2)	
	$M_S \geq 6.2$	$M_w = M_S$	(3)	Scordilis (2006)
$m_b$	$3.5 \leq m_b \leq 6.2$	$M_w = 0.85(\pm 0.04)m_b + 1.03(\pm 0.23)$	(4)	

existing uncertainties have been identified and reduced as much as possible. Seismic hazard maps of Kerman province have been developed in term of PGA and spectral acceleration (SA) intensity measures with 5% damping for 2% and 10% probability of exceedance in 50 years. This paper used the classic PSHA method (like the Cornell, 1968) to meet design requirements based on Iranian seismic design code (Standard NO. 2800). Due to the severe uncertainties in the properties of substructure soil and the need for detailed geotechnical studies on the site, where the structure was constructed, as well as the necessity to compare the resulting maps with those existing in the mentioned codes, it was decided not to consider the local site effects. Therefore, results are presented for bedrock condition.

### 3.2 Data

In the first stages of this research, authors compiled an integrated catalog of the earthquakes which occurred in the area. Instrumental recording of earthquakes has been initiated since the early twentieth century. Iranian earthquakes are mainly reported by the Iranian Seismological Center (IRSC, IGUT) and the International Institute of Earthquake Engineering and Seismology of Iran (IIEES), respectively in Nuttli ( $M_N$ ) and Local ( $M_l$ ) magnitudes. The main catalog used in this study is related to data recorded by the IRSC. Due to the lack of seismic stations in different parts of Iran and the fact that not all earthquakes were recorded in the early years of the establishment of the local seismic network of Iran, complementary data available from the international seismic networks was used to complete the seismic catalog. The main data, obtained from international seismic networks, are the events recorded by the International Seismological Centre (ISC), the National Earthquake Information Center (NEIC), and the Global Centroid-Moment-Tensor (GCMT) of Harvard University. Historical catalogs compiled by Ambraseys and Melville (1982), and Berberian (1994) were used to complete the historical catalog and to account for events before 1900.

In the next step, to integrate the magnitudes, all magnitudes were changed to moment magnitude, because the

moment magnitude is not saturated (Idriss, 1985). The relationships used to convert the magnitudes are given in Table 2 (Karimiparidari et al., 2013; Nemati & Tatar, 2015; Scordilis, 2006; Stirling et al., 2013). Due to the saturation of the body-wave magnitude ( $m_b$ ) at an approximate magnitude of 6.2 (Scordilis, 2006), conversion by the surface wave magnitude ( $M_s$ ) was a priority, especially for large magnitudes. Using  $m_b$  to convert magnitudes greater than 6.2 is one source of uncertainty in the seismic catalog, which due to its direct relationship to seismic parameters, severely affects the b-value (one of the coefficients of the Gutenberg-Richter recurrence law) as will be show in Eq. 5. Therefore, in order to reduce the uncertainties caused by the magnitude conversions in the catalog and also to reduce the spatial uncertainties (epicentral location and depth of events), the algorithm presented in the Fig. (2) was utilised by authors to convert the magnitudes. The uncertainties in the epicentral location and depth of events are directly related to the modeling of Seismic Zones (SSZs).

## 4 Results

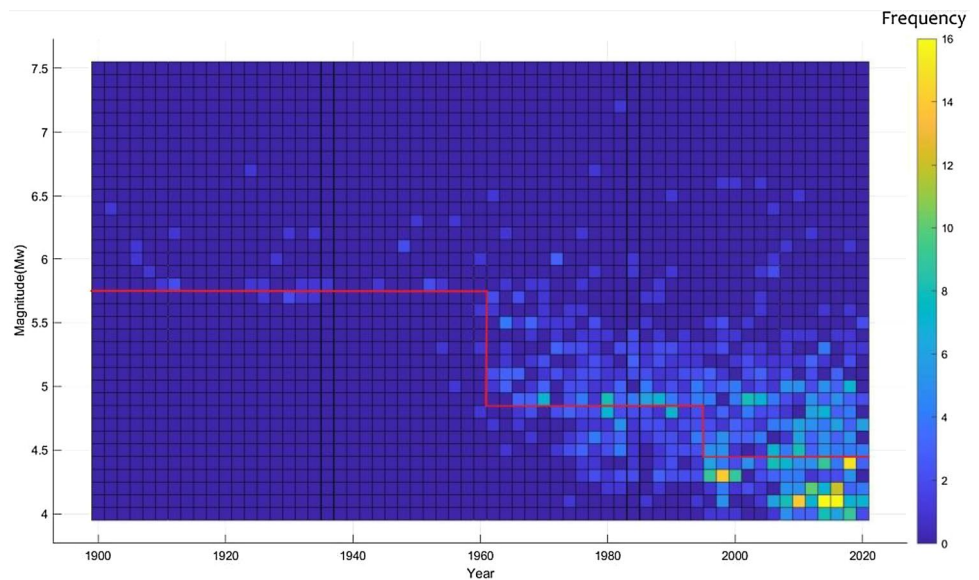
To provides probabilistic seismic hazard analysis of Kerman province with emphasis on uncertainties in different steps of analysis; we explained and reviewed the results of our analysis on the seismicity parameters and uncertainties, foreshocks and aftershocks removing, magnitude conversion uncertainty, catalog completeness, Seismic source models, and Ground Motion Predictive Models.

### 4.1 Seismicity parameters and uncertainties

One of the key and most important steps in PSHA is estimating the seismicity parameters: the Gutenberg-Richter recurrence law (Eq. 5),  $M_{\min}$ ,  $M_{\max}$  and activity rate  $\lambda$

$$\log \lambda_m = a + bM \quad (5)$$

where,  $\lambda_m$  is the mean annual rate of exceedance from magnitude  $M$ ,  $10^4$  is the mean yearly number of earthquakes corresponding to  $M_{\min}=0$  and b-value express the relative likelihood of large and small events. A decrease in b-value indicates an increase in the number of large earthquakes

**Fig. 3** Histogram of catalog completeness

compared to small ones in each SSZ. Seismic analysis have high uncertainties. There are two types of uncertainties: inherent or intrinsic and epistemic uncertainties. Intrinsic uncertainties arise from the natural characteristics of the earthquake process, and are inevitable. However, epistemic uncertainties are due to the incompleteness of the knowledge about this process (Gaspar-Escribano et al., 2015) which should be addressed. All the uncertainties associated with the seismicity parameters are epistemic. Before determining seismicity parameters, the seismic catalog must be refined and the sources of uncertainties in the measurement of these parameters have to be identified.

#### 4.2 Foreshocks and aftershocks removing

The purpose of PSHA is to investigate the hazard of independent events. In some areas, seismicity may be distorted by dependent events such as foreshocks and aftershocks (Merz & Cornell, 1974), and disrupt the Poisson distribution of earthquakes in the Gutenberg-Richter law. Therefore, dependent events should be removed from the seismic catalog before calculating the seismicity parameters. Thus, different declustering algorithms (e.g. Gardner & Knopoff, 1974; Hainzl et al., 2006; Reasenber, 1985; Zhuang et al., 2002) have been proposed. In the present study, Gardner and Knopoff (1974) time–space windows method was used to remove dependent events from the catalog.

#### 4.3 Magnitude conversion uncertainty

Inappropriate magnitude conversion relationships can lead to 33% and 42% uncertainty in  $a$ , and  $b$ -value (Eq. 5), respectively (Das et al., 2020). Since the relationship between the moment magnitude to other magnitude is extracted from

the regression of the data recorded in both magnitudes, and small earthquakes that occurred in Iran are not reported with the moment magnitude, then the relationships developed to convert Nuttli to moment magnitude has more uncertainty in lower magnitude than higher magnitudes. It will cause more uncertainty in the determination of seismicity parameters. Between 2006 and 2020 (Fig. 3), data were taken from local seismic stations, and the origin of the magnitude of events is Nuttli (1973); Therefore, events with  $4.0 \leq M_w \leq 4.5$  have been affected by the conversion relationship and caused overestimation in seismicity results. Thus,  $M_{\min}$  was identified as another source of uncertainty in this study. Increasing  $M_{\min}$  reduces the results of the PGA in low to moderate return periods (Baker, 2008). In PSHA analysis, only the events with a moment magnitude larger than 4.0 or 5.0, which are able to cause significant damage to the structure, are important. Therefore, the appropriate  $M_{\min}$  for this research was considered as 4.5. In addition to the  $M_{\min}$ , factors such as the priority of using  $M_s$  over  $m_b$  to convert magnitudes has a significant impact on seismicity parameter results as discussed earlier in the catalog refinement section. Due to the uncertainties in the magnitude conversion relationships, use of two successive conversion relationships to convert origin to moment magnitude is another source of uncertainty that should be avoided.

#### 4.4 catalog completeness

In the past, the lack of seismic stations and the low sensitivity of seismographs in the area have led to some events not being recorded. Therefore, data with a magnitude less than a threshold magnitude is incomplete at different time intervals. Affecting this defective data in the determination of seismicity parameters causes an underestimation

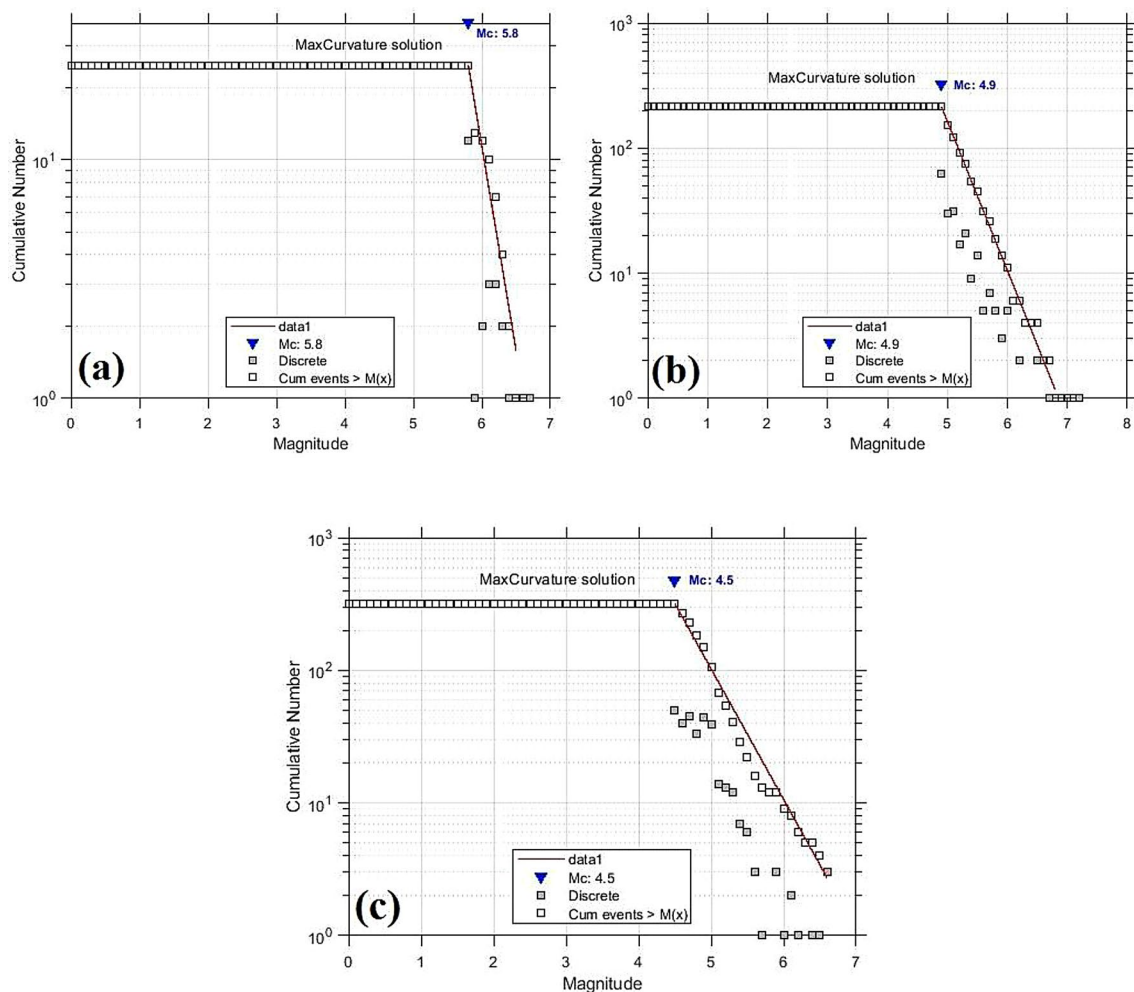


**Fig. 4** Magnitude completeness estimation using Maximum Curvature method for time intervals of **a** 1900–2020, **b** 1960–2020, and **c** 1996–2020

and uncertainty in seismicity parameters. The incomplete data must be removed from the seismic catalog, and the threshold magnitude, which is called the completeness of magnitude, must be specified for different time intervals in the catalog. Due to the establishment and increase in the number of seismic stations and the improvement of analysis methods, the magnitude of completeness in the catalog of an area is usually reduced over time. In this study, the Stepp (1973) method was used to investigate the magnitude of completeness in different time intervals. Assuming that, the events have a Poisson distribution, as magnitude decreases, the number of events increases; therefore, the decrease in the number of events indicates an incomplete recording of events in the relevant time interval. In the present study, to investigate the time intervals of completeness, the histogram of the year was plotted against the magnitude for earthquakes larger than 4.0 and magnitudes of completeness estimated (Fig. 3). Finally, by using ZMAP software package, according to the maximum curvature-method,

the magnitude of completeness of 5.8, 4.9, and 4.5 was obtained for 1900–2020 (Fig. 4a), 1960–2020 (Fig. 4b), and 1996–2020 (Fig. 4c) time intervals, respectively, which were the same as those show in Fig. 3. Therefore, the data below the red line in Fig. 3 was removed from the catalog. Previously, Mousavi-Bafrouei et al. (2014) proposed 1900-present, 1964-present, and 1997-present intervals to determine the magnitude of completeness throughout Iran. In practical engineering projects throughout Iran, only two intervals, 1900-present and 1963-present, are usually considered. It is recommended that in these analyzes, instead of considering these two intervals, the three intervals be used to determine the magnitude of completeness.

The method proposed by Kijko et al. (2016) was used to calculate the seismicity parameters. Table 3 lists the seismicity parameters of all the 21 SSZs. All historical and instrumental events were applied to determine seismicity parameters. In this the current study,  $M_{\max}$  was considered



**Table 3** Seismicity parameters of all 21 seismic source zones

Source Zone Number	Seismicity Parameters						
	$M_{min}$	$M_{max}$	$\lambda_{4,5}$	$a$	$b$	$\sigma(b)$	
1	4.5	6.7	0.74	4.91	1.12	0.05	
2	4.5	5.8	0.21	3.82	1.00	0.06	
3	4.5	7.1	0.26	4.05	1.03	0.06	
4	4.5	7.7	0.66	4.14	0.96	0.05	
5	4.5	6.4	0.67	4.37	1.01	0.06	
6	4.5	6.6	0.26	4.10	1.04	0.05	
7	4.5	6.0	0.29	4.01	1.01	0.06	
8	4.5	7.1	1.13	4.82	1.06	0.05	
9	4.5	7.2	0.88	4.17	0.94	0.05	
10	4.5	6.7	0.33	4.15	1.03	0.05	
11	4.5	6.3	0.10	3.50	1.00	0.05	
12	4.5	6.9	0.26	4.00	1.02	0.05	
13	4.5	6.7	0.44	4.28	1.03	0.06	
14	4.5	6.7	0.63	4.16	0.97	0.05	
15	4.5	6.7	0.97	4.58	1.02	0.05	
16	4.5	7.0	1.07	4.93	1.09	0.05	
17	4.5	6.3	0.24	3.97	1.02	0.05	
18	4.5	7.2	0.50	4.38	1.04	0.05	
19	4.5	5.7	0.19	3.82	1.01	0.06	
20	4.5	5.8	0.45	4.38	1.05	0.06	
21	4.5	7.5	0.27	3.71	0.95	0.05	
1	4.5	6.7	0.74	4.91	1.12	0.05	

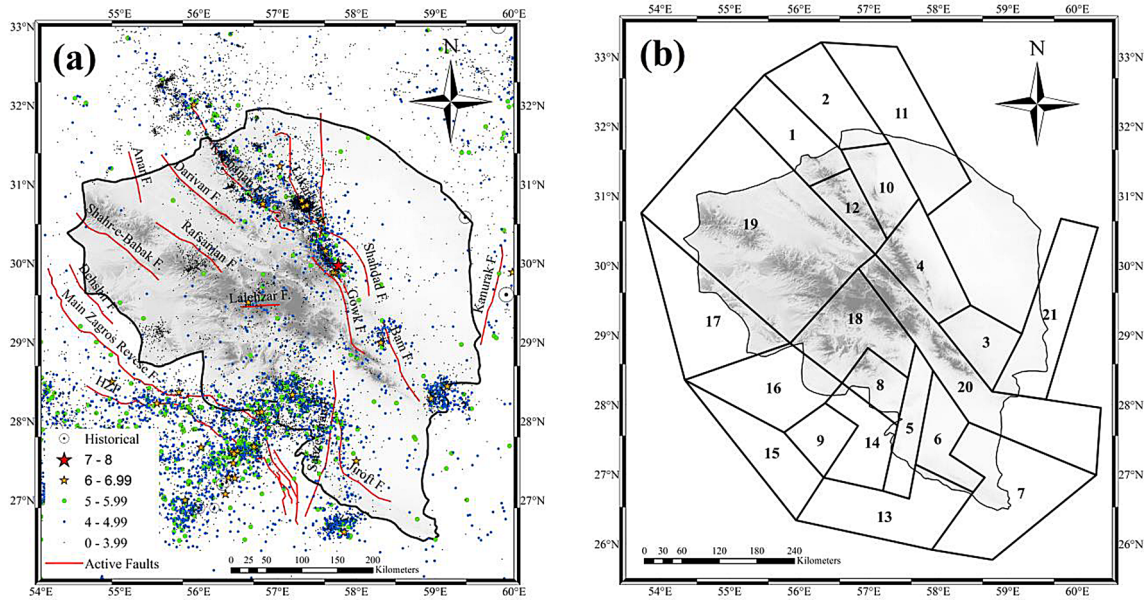


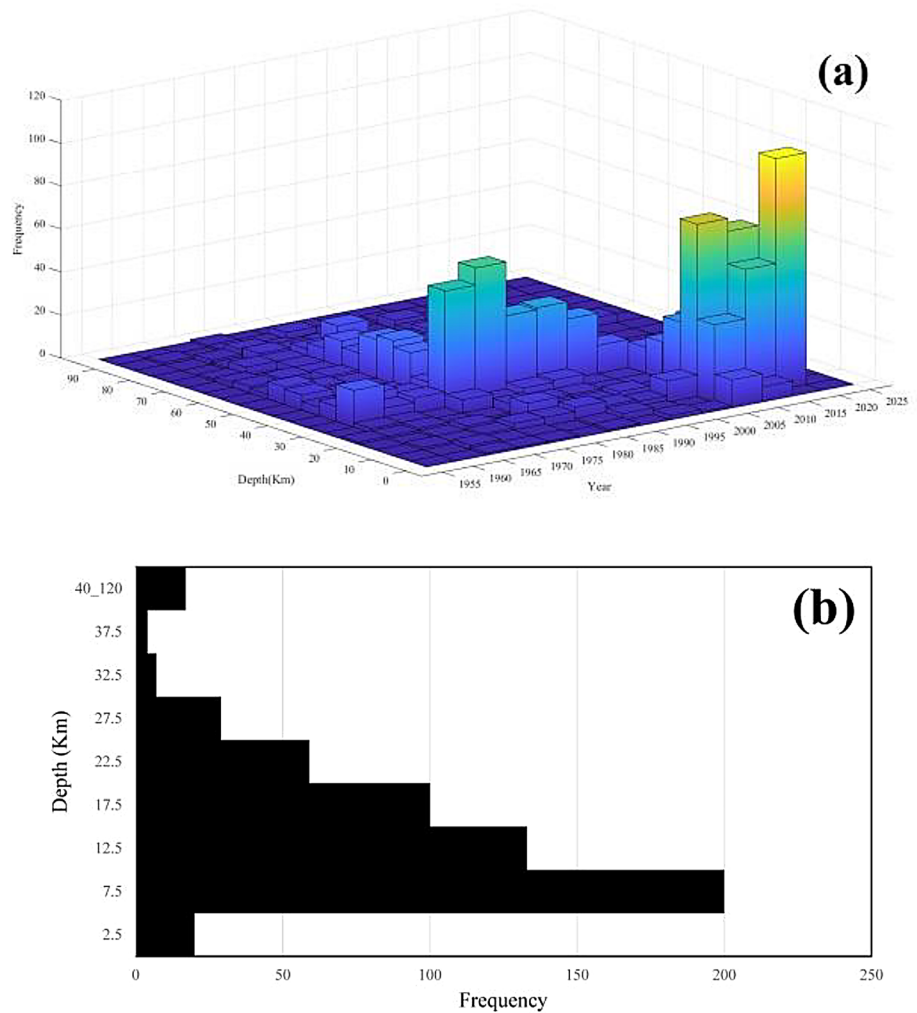
**Fig. 5** a Distribution of earthquake events throughout Kerman province and its around area. b Seismic source zones in the area

half a unit higher than the largest historical and instrumental event in each SSZ.

### 4.5 Seismic source models

Seismic source zone (SSZ) modeling can produce very different results due to judgment and interpretation of

**Fig. 6 a** Diagram of the earthquake events depth—date (years) in the Kerman province. The diagram show that the depth of events recorded in the region sharply decreased after 2005. **b** Diagram of the earthquake events depth- frequency for the  $M_w \geq 4.5$  events recorded in the Kerman province by local seismic stations. According to this diagram, more than 86% of the recorded events in the region have occurred between 5 to 25 km. More than 35% of these events occurred in the range of 5 to 10 km. The earthquakes depth in all SSZs is considered to be 7.5 km



insufficient data (Gülerce & Vakilinezhad, 2015). In the study area, only the events related to the Lakarkuh, Bam, Sirch-Golbaf and Kouhbanan faults have been well recognized on their segments, and the other events have been referred to the any other faults, based on speculations. One method of modeling SSZs for large-scale areas including unknown faults is the use of areal SSZs (Abrahamson, 2006; Maiti & Kamai, 2020). Figure 5a shows the distribution of earthquakes in Kerman province. Due to the scattering of data, the uncertainty of the epicentral location of events, the fault recognition, and the impossibility of relating events to active and known faults in the area, it was decided that all SSZs were considered areal. In the present PSHA analysis, the distribution of earthquakes in SSZs is assumed to be uniform, so efforts were made to ensure that all areas within each SSZ had the same seismic characteristics as possible. In the process of modeling SSZs, four criteria of faults location, seismicity, focal mechanism, and geological conditions were considered for the definition of SSZs from each other, and finally, 21 SSZs were specified for the region (Fig. 5b).

In modeling, SSZs up to a radius of at least 150 km from the sites were identified. In the process of SSZs identifying, in addition to the four criteria mentioned above, sufficient data to determine the seismicity parameters of each SSZ as a limiting factor prevented the separation of SSZs from each other on a smaller scale. Also, the uncertainty in the depth of the events was considered. The depth of events that reported by regional networks in Iran has an uncertainty of more than 20 km (Maggi et al., 2002). Therefore, for the present study, investigations were carried out on the depth of the events in the region. Figure 6a shows a diagram of the year vs the depth of events in the Kerman region. According to this diagram, it can be concluded that the depth of events recorded in the study area has sharply decreased since 2005. The reason for the sudden decrease in the depth of events is that the data used in this section of the catalog is entirely derived from the IRSC local seismic network. Therefore, another source of uncertainty in PSHA analysis on the Iranian plateau is the use of depths recorded by non-local seismic networks. Finally, it was decided to use only the data

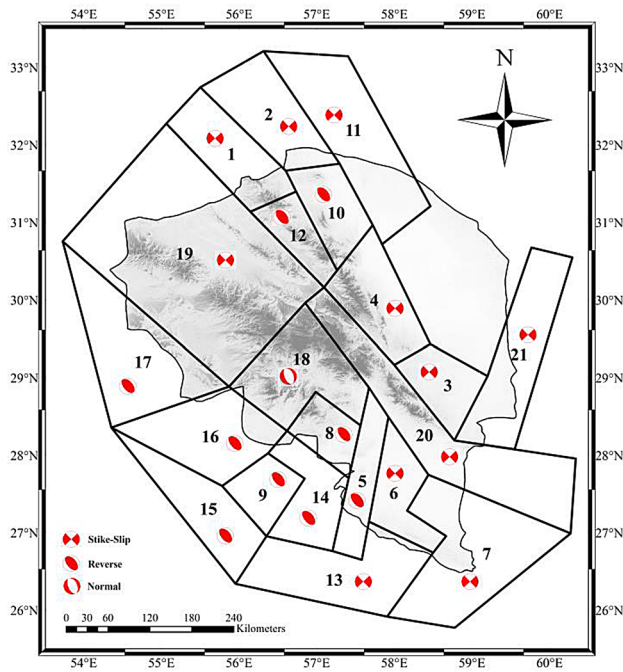


**Fig. 7** Dominant focal mechanism of seismic source zones in the Kerman province and its around area

recorded by the local IRSC seismic network to investigate the depth of events. Figure 6b shows the frequency diagram of events greater than 4.5 against depth for data recorded by local seismic networks in the Kerman region. According to this chart, more than 86% of the recorded events in the region have occurred between 5 and 25 km. More than 35% of these events occurred in the 5–10 km range. Therefore the depth of earthquakes in all SSZs is considered to be 7.5 km. The focal mechanism of all 21 identified SSZs was specified according to the dominant focal mechanism in each SSZ. For SSZs that did not have enough focal mechanism data, decisions were made according to the SSZs around them and the corresponding mechanism of their nearby faults. The faults studied in this research were derived from Hesami and Jamali (2006) for which, the focal mechanisms were plotted using GCMT catalog (Dziewonski et al., 1981; Ekström et al., 2012) and 3D focal mechanism software Package. The predominant mechanism of SSZs is shown in Fig. 7.

#### 4.6 Ground motion predictive models

Ground-Motion Predictive Models (GMPMs) estimate the intensity measures (such as PGA and SA) for a particular site, taking into account the effects of the source, the source-to-site path, and the site condition (Sucuoğlu & Akkar, 2013). GMPMs are usually based on empirical relationships

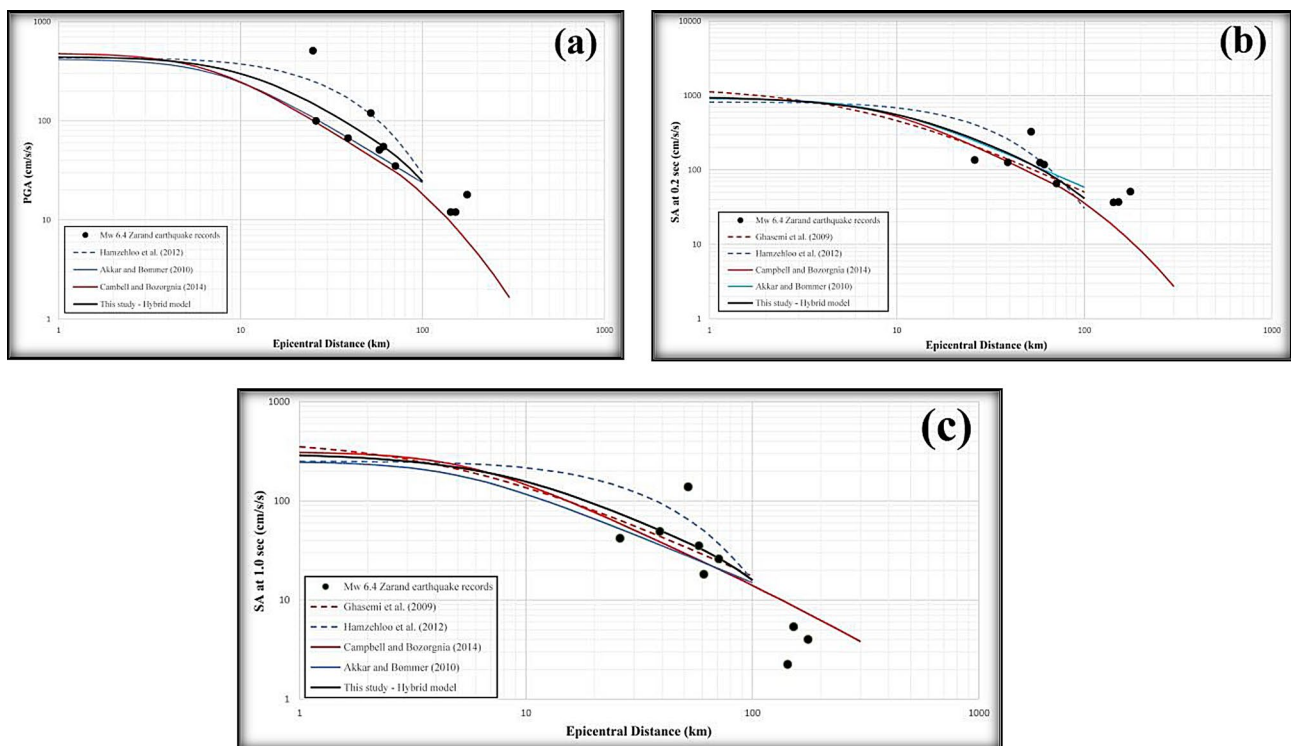


**Fig. 8** Comparison of the Mw 6.4 Zardand earthquake data with GMPE used in this study for **a** PGA, **b** SA at 0.2 s and **c** SA at 1.0 s

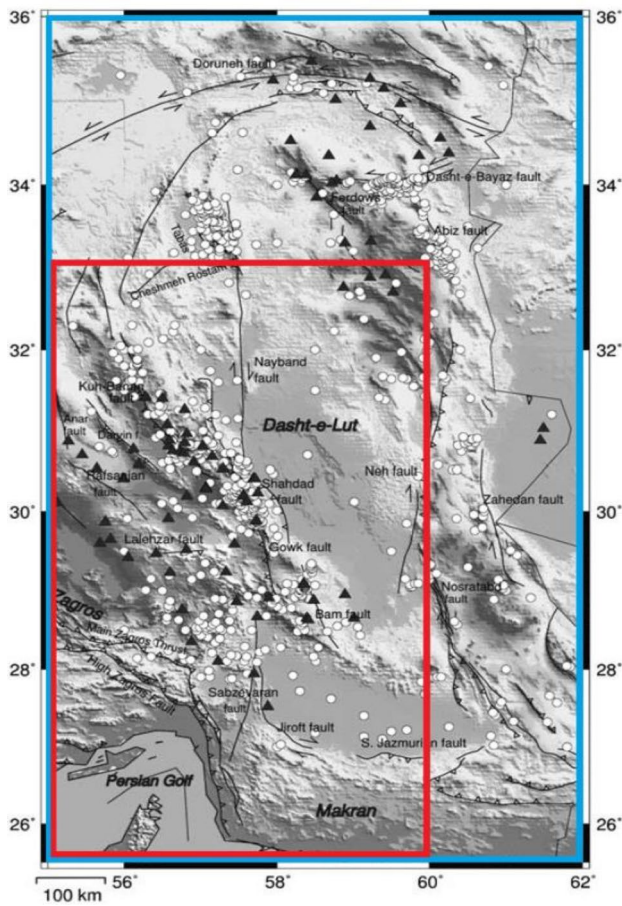


**Fig. 9** GMPE frame of this study’s area (red rectangle) and Hamzehloo and Mahood (2012) (blue rectangle). Triangles indicate strong ground-motion stations and circles indicate earthquakes occurred between 1978 and 2008

and regression on a set of ground motion data. The general form of a GMPE relationship is given in Eq. (6).

$$\ln Y = f(M) + f(R) + f(FM) + f(LSE) \tag{6}$$

where  $\ln Y$  represents the desired ground motion parameter (such as PGA), and  $f(*)$  terms, indicate the magnitude, distance of the source-to-site, faulting mechanism, local site effect, respectively. The effects of the source are considered by the two variables of magnitude (M) and faulting mechanism (FM), the effects of the path by the site-to-source distance (R), and the effects of the site condition by the local site effect (LSE). Until now, several GMPMs have been developed for Iran plateau (Amiri et al., 2007; Ghasemi et al., 2009; Hamzehloo & Mahood, 2012; Safari et al., 2012; Yazdani & Kowsari, 2013b; Zafarani et al., 2018). Due to the proximity of the 2005 Zarand earthquake to the seismological stations of the BHRC, with 6 and 17 records in less than 40 km and 100 km distance, respectively, this earthquake is considered as the best event recorded by accelerographs in Kerman region. Therefore, to validate selected GMPMs and to use then in this study, models were compared with the records of the 2005 Zarand earthquake, which were obtained on bedrock condition (Fig. 8). Then, according to the four selected GMPMs, a hybrid model was developed to use in this analysis.

A hybrid GMPM is a weighed combination of two or more distributions, which can assign different mean values, standard deviations to the analyzed data (Scherbaum et al., 2005). Conditional probability of exceedance of an intensity measure, A, is calculated using:

$$P(A > a) = \sum_{i=1}^N w_i \left\{ 1 - \phi \left[ \frac{a - \mu_i}{\sigma_i} \right] \right\} \tag{7}$$

where  $w_i$  is the weight of the  $i^{th}$  initial GMPM,  $\phi \left[ \frac{a - \mu_i}{\sigma_i} \right]$  is the normal distribution. The  $\sigma_i$  and  $\mu_i$  are the standard deviations and mean values of the  $i^{th}$  initial GMPM, respectively.

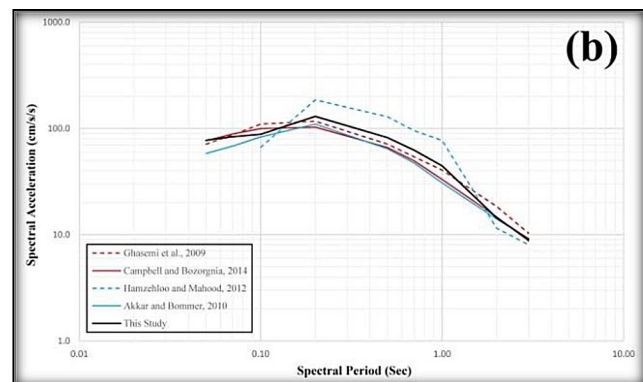
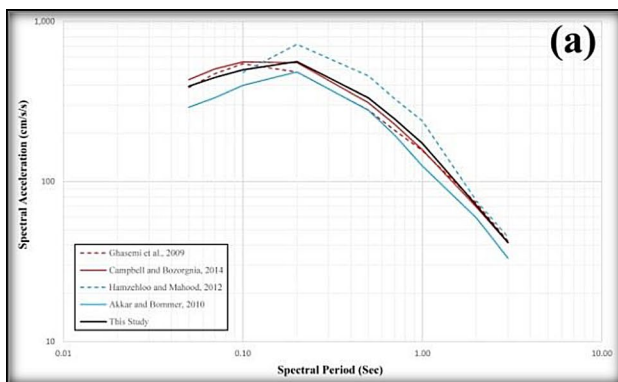


**Fig. 10** Comparison between selected GMPEs and the hybrid model developed in this study for a Strike-Slip Mw 6.5 earthquake at distance of a 10 km b 50 km

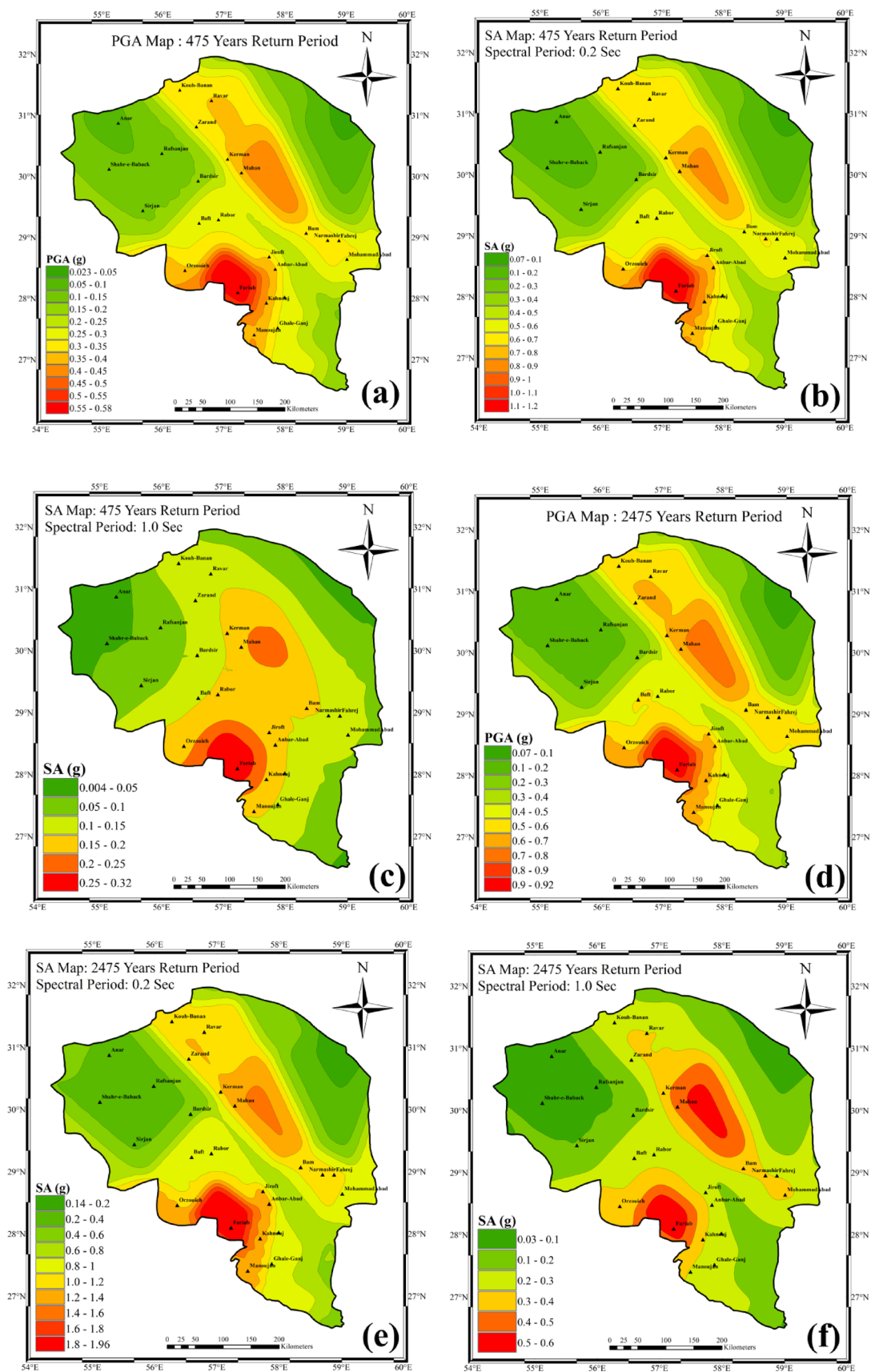


Fig. 11 Seismic hazard maps for PGA and SA in return periods of a–c 475 years d–f 2475 years for Kerman province

According to Ordaz and Arroyo (2016), the results of both logic tree and Hybrid GMPM methods are the same.

The characteristics of the selected GMPMs are as follows:

(1) Hamzehloo and Mahood (2012): To compile this GMPM, the data of East-Central Iran has been used; therefore, it was considered one of the most suitable GMPMs for this research. Figure 9 shows this study's area and the area for which Hamzehloo and Mahood (2012). This GMPM has been developed for bedrock site condition ( $V_s = 760$  m/s) by considering two variables of site-to-source distance and magnitude. This GMPM is developed for the PGA and Spectral Acceleration (SA) (0.1s–5s spectral periods) and is applicable to earthquakes with  $M_w$  5.0–7.4 and having distance within the range of 1–100 km.

(2) Ghasemi et al. (2009): This relationship has been developed using data from Iran and Western Eurasia for the SA in the range of 0.05s to 3s. In this GMPM, the range of magnitude and distance is  $M_w$  5.0 to 7.4 and distance 0.5 to 100 km, respectively.

(3) Akkar and Bommer (2010): This GMPM has been compiled using data from Middle Eastern and European earthquakes for PGA, SA and PGV intensity measures in the range of 0.0–3.0 S. spectral periods and applies to  $M_w$  5.0–7.6 and up to 100 km. Focal mechanism has been considered in this GMPM.

(4) Campbell and Bozorgnia (2014): This GMPM was developed using global data for evaluation of ground motion parameters such as PGA, PGV, and SA for 0–10 S. periods and is useful in 0–300 km and 3.0–8.5 intervals of distance and moment magnitude, respectively. In this GMPM, the style of faulting and local site effects have also been considered. Ghasemi et al. (2008) using LLH test indicated the Campbell and Bozorgnia (2008) GMPM is one of the most appropriate models to use on the Iranian plateau. The authors used an update of this relationship for this study, Campbell and Bozorgnia (2014).

The relationship developed by Hamzehloo and Mahood (2012) has a very high fit with the study area, despite the use of less data than other GMPMs. On the other hand, although a small percentage of the region's data is used to formulate Campbell and Bozorgnia (2014) GMPM, the use of global data covers a wide range of magnitude, distance, and spectral period. Also, in the presence of sufficient data in this GMPM, the site effects and focal mechanisms are well-considered. Each of the above GMPMs has its benefits; therefore, the hybrid model has been developed with the same weighting for all four GMPMs. Figure (10) shows the Preferred GMPMs compared to the hybrid model developed for this study, for a strike-slip  $M_w = 6.5$  earthquake at 10 km (Fig. 10a) and 50 km (Fig. 10b) away.

## 4.7 PSHA maps

Seismic hazard maps are one of the basic needs for seismic codes; therefore, updating such maps will lead to a more reliable seismic design. Such maps can be used to prioritize metropolitan planning, strategies, and policies (Yazdani & Kowsari, 2017). Attempts were made in this study to consider as much as possible the uncertainties in each of the PSHA steps, including catalog refinement, SSZs modeling, seismicity parameters and GMPMs. The algorithm developed to compile the catalog presented in this study can be used to reduce the epistemic uncertainties of the seismic catalog which are based on IRSC data. In this study, to increase the accuracy of the analysis, the identified SSZs were considered as small as possible from previous research. In identification of these SSZs, five criteria including, seismicity, faults, focal mechanisms, geological conditions, and sufficient data for each SSZ (as a limiting factor) were applied. In this study, the minimum magnitude and uncertainty of magnitude conversion relationships in lower magnitudes were also identified as the causes of uncertainty in the results of PSHA, which should be examined in detail in independent research. Finally, the combination of different GMPMs, the use a hybrid model instead of the logic tree, the time required for analysis is significantly reduced due to the combination of GMPMs before analysis and the creation of a new GMPM based on selected GMPMs. In Fig. 11, seismic hazard maps with a probability of 2% and 10% probability of exceedance in 50 years for the SA in spectral periods of 0.2 s and 1.0 s and the PGA parameter corresponding to 5% damping calculated for  $13 \times 13$  km ( $0.06^\circ \times 0.06^\circ$ ) blocks are presented. The PGA values for the 475-year return period (Fig. 11a) for the densely populated cities in Kerman province, including Kerman, Jiroft, Sirjan, Rafsanjan, and Bam, were estimated at 0.35 g, 0.35 g, 0.15 g, 0.15 g, and 0.35 g, respectively. These values are comparable to those provided by existing studies (Mahsuli et al., 2019; Mohammadi & Bayrak, 2016; Moinfar et al., 2012). The highest PGA with the same return period was estimated to be 0.58 g in the city of Faryab, which is located near the interaction of Zagros, Central Iran and Makran plates. The lowest PGA values with the same return period is also related to the uninhabited area of Lut plain and Anar city, which are 0.05 and 0.1g, respectively.

The maximum PGA for 2475 years return period (Fig. 11d) for the cities of Kerman, Jiroft, Sirjan, Rafsanjan, and Bam was estimated at 0.6 g, 0.6 g, 0.3 g, 0.2 g, and 0.6 g, respectively. The minimum and maximum PGA with the same return period is related to the non-residential area of Lut plain and Faryab city, which is estimated to be 0.1 g and 0.92 g, respectively. Spectral acceleration values for spectral periods of 0.2 s (Fig. 11b, e) and 1 s (Fig. 11c, f) in 475 and 2475 years return periods are also provided to meet the design requirements of spectral acceleration-based codes.

The merit of the current study and the principal difference between this study and other studies carried for Kerman province (Dehghan-Manshadi et al., 2020; Saafi-zaadeh & Bagheripour, 2019) are: (1) The present study carried the first PSHA analysis extending the area of study to whole Kerman province, while previous studies have covered only part of this area; (2) In this study local attenuation relationships were applied, for the first time, to provide a seismic hazard map for this region; and (3) The spectral acceleration maps presented here are the first maps developed for this region.

## 5 Discussion and conclusion

This research presents the seismic hazard maps of Kerman province, which have been developed in term of PGA and spectral acceleration (SA) intensity measures with 5% damping for 2% and 10% probability of exceedance in 50 years. We used the classic PSHA method, to meet design requirements based on Iranian seismic design code (Standard NO. 2800).

In the 475-year return period, the PGA values for the densely populated cities in Kerman province, including Kerman, Jiroft, Sirjan, Rafsanjan, and Bam, were estimated at 0.35 g, 0.35 g, 0.15 g, 0.15 g, and 0.35 g, respectively. The highest and lowest PGA with the same return period were estimated 0.58 g and 0.05g in the Faryab city, and the Lut plain, respectively.

In the 2475 years return period, the maximum PGA for the cities of Kerman, Jiroft, Sirjan, Rafsanjan, and Bam was estimated at 0.6 g, 0.6 g, 0.3 g, 0.2 g, and 0.6 g, respectively. The maximum and minimum PGA with the same return period are related to the Faryab city and Lut plain, which were estimated 0.92 g and 0.1 g, respectively.

**Acknowledgements** This work was supported by the Shahid Bahonar University of Kerman in Kerman, Iran. Thanks the editor, and two anonymous reviewers for helpful reviews of this manuscript. Grateful to the Dr. Milad Kowsari for his comments and insightful suggestions and careful reading of the manuscript. We appreciate Maryam Sadeghi's advice and guidance.

**Data and resources** Data for seismic catalog compilation were mainly obtained from the Iranian Seismological Center (IRSC), <http://irsc.ut.ac.ir/bulletin.php> (last accessed January 2020), the International Seismological Centre (ISC), <http://www.isc.ac.uk/iscbulletin/search/bulletin/> (last accessed January 2020), the National Earthquake Information Center (NEIC), <https://earthquake.usgs.gov/earthquakes/search/> (last accessed January 2020), and the Global Centroid Moment Tensor (GCMT), <https://www.globalcmt.org/CMTsearch.html> (last accessed January 2020), databases. Data on the focal mechanism were taken from the GCMT catalog, <https://www.globalcmt.org/CMTsearch.html> (last accessed January 2020). Data on earthquake accelerometers were obtained from Building and Housing Research Center (BHRC), <https://>

[smd.bhrc.ac.ir/Portal/en/Search/Waveforms](https://smd.bhrc.ac.ir/Portal/en/Search/Waveforms) (last accessed March 2020).

## References

- Abrahamson, N. A. (2006). Seismic hazard assessment: problems with current practice and future developments. In: First European Conference on Earthquake Engineering and Seismology, pp. 3–8.
- Akkar, S., & Bommer, J. J. (2010). Empirical equations for the prediction of PGA, PGV, and spectral accelerations in Europe, the mediterranean region, and the Middle East. *Seismological Research Letters*, 81, 195–206. <https://doi.org/10.1785/gssrl.81.2.195>
- Ambraseys, N. N., & Melville, C. P. (1982). *A history of Persian earthquakes* (p. 100). Cambridge University Press.
- Ambraseys, N. N., & Melville, C. P. (2005). *A history of Persian earthquakes*. Cambridge University Press.
- Amiri, G. G., Mahdavian, A., & Dana, F. M. (2007). Attenuation relationships for Iran. *Journal of Earthquake Engineering*, 11, 469–492. <https://doi.org/10.1080/13632460601034049>
- Baker, J. W. (2008). *An introduction to probabilistic seismic hazard analysis (PSHA)*. Citeseer.
- Berberian, M., 1994. Natural Hazards and the first earthquake catalog of Iran. *Geol. Surv. Iran*.
- Berberian, M. (2014). Earthquakes and Coseismic Surface Faulting on the Iranian Plateau. Available Online: <https://www.worldcat.org/isbn/9780444632920/> [20 June 2014]
- Berberian, F., & Berberian, M. (1981). Tectono-plutonic episodes in Iran. In H. K. Gupta & F. M. Delany (Eds.), *Zagros-Hindu Kush-Himalaya geodynamic evolution* (Vol. 3, pp. 5–32). Am. Geophys. Union, Geodynamics Series.
- Berberian, F., Muir, I. D., Pankhurst, R. J., & Berberian, M. (1982). Late cretaceous and early miocene andean-type plutonic activity in northern makran and Central Iran. *Journal of the Geological Society*, 139, 605–614.
- Berberian, M., Jackson, J. A., Qorashi, M., & Kadjar, M. H. (1984). Field and teleseismic observations of the 1981 Golbaf-Sirch earthquakes in SE Iran. *Geophysical Journal International Astronomy Society*, 77, 809–838.
- Berberian, M., & Qorashi, M. (1994). Coseismic fault-related folding during South Golbaf earthquake of November 20, 1989, in southeast Iran. *Journal of Geology*, 22, 531–534.
- Berberian, M., Qorashi, M., Jackson, J. A., Fielding, E., Parsons, B. E., Priestley, K., Talebian, M., Walker, R., Wright, T. J., & Baker, E. (2001). The 1998 March 14 Fandoqa earthquake M = 6.6 in Kerman, southeast Iran: Re-rupture of the 1981 Sirch earthquake fault, triggering of slip on adjacent thrusts, and the active tectonics of the Gowk fault zone. *Geophysical Journal of International*, 146(2), 371–398.
- Campbell, K. W., & Bozorgnia, Y. (2008). NGA ground motion model for the geometric mean horizontal component of PGA, PGV, PGD and 5% damped linear elastic response spectra for periods ranging from 0.01 to 10 s. *Earthquake Spectra*, 24, 139–171. <https://doi.org/10.1193/1.2857546>
- Campbell, K. W., & Bozorgnia, Y. (2014). NGA-West2 ground motion model for the average horizontal components of PGA, PGV, and 5% damped linear acceleration response spectra. *Earthquake Spectra*, 30, 1087–1114. <https://doi.org/10.1193/062913EQS175M>
- Cornell, B. Y. C. A. (1968). Owing to the uncertainty in the number, sizes, and locations of future earthquakes it is appropriate that engineers express seismic risk, as design winds or floods are, in terms of return periods (Blume, 1965; Newmark, 1967; Blume, Newmark and C. Bulletin of the Seismological Society of America, 1583–1606.

- Das, R., Gonzalez, G., de la Llera, J. C., Saez, E., Salazar, P., Gonzalez, J., & Meneses, C. (2020). A probabilistic seismic hazard assessment of southern Peru and Northern Chile. *Engineering Geology*, 271, 105585. <https://doi.org/10.1016/j.enggeo.2020.105585>
- Dehghan-Manshadi, S. H., Mirzaei, N., Eskandari-Ghadi, M., Shabani, E., & Mousavi-Bafrouei, S. H. (2020). Time-dependent probabilistic seismic hazard assessment in Kerman and adjacent areas in the west of Lut block, Central-East Iran. *Bulletin of Engineering Geology and the Environment*, 79, 5079–5094. <https://doi.org/10.1007/s10064-020-01897-6>
- Dziewonski, A. M., Chou, T. A., & Woodhouse, J. H. (1981). Determination of earthquake source parameters from waveform data for studies of global and regional seismicity. *Journal of Geophysical Research*, 86, 2825–2852. <https://doi.org/10.1029/JB086iB04p02825>
- Ekström, G., Nettles, M., & Dziewoński, A. M. (2012). The global CMT project 2004–2010: Centroid-moment tensors for 13,017 earthquakes. *Physics of the Earth and Planetary Interiors*, 200–201, 1–9. <https://doi.org/10.1016/j.pepi.2012.04.002>
- Ezati, M., Gholami, E., Mousavi, S. M., Rashidi, A., & Derakhshani, R. (2022a). Active Deformation Patterns in the Northern Birjand Mountains of the Sistan Suture Zone, Iran. *Applied Sciences*, 12, 6625. <https://doi.org/10.3390/app12136625>
- Ezati, M., Rashidi, A., Gholami, E., Mousavi, S. M., Nemati, M., Shafieibafti, S., et al. (2022b). Paleostress analysis in the Northern Birjand, East of Iran: Insights from inversion of fault-slip data. *Minerals*, 12, 1606. <https://doi.org/10.3390/min12121606>
- Fielding, E. J., Talebian, M., Rosen, P. A., Nazari, H., Jackson, J. A., Ghorashi, M., & Walker, R. (2005). Surface ruptures and building damage of the 2003 Bam, Iran, earthquake mapped by satellite synthetic aperture radar interferometric correlation. *Journal of Geophysical Research*, 110, B03302. <https://doi.org/10.1029/2004JB003299>
- Foroutan, M., et al. (2014). Late Pleistocene-Holocene right slip rate and paleo-seismology of the Nayband fault, western margin of the Lut block, Iran. *Journal of Geophysical Research: Solid Earth*, 119(4), 3517–3560.
- Gardner, J. K., & Knopoff, L. (1974). Is the sequence of earthquakes in Southern California, with aftershocks removed, Poissonian? *Bulletin of the Seismological Society of America*, 64, 1363–1367.
- Gaspar-Escribano, J. M., Rivas-Medina, A., Parra, H., Cabañas, L., Benitoa, B., Ruiz Barajas, S., & Martínez Solares, J. M. (2015). Uncertainty assessment for the seismic hazard map of Spain. *Engineering Geology*, 199, 62–73. <https://doi.org/10.1016/j.enggeo.2015.10.001>
- Ghasemi, H., Zare, M., & Fukushima, Y. (2008). Ranking of several ground-motion models for seismic hazard analysis in Iran. *Journal of Geophysics and Engineering*, 5, 301–310. <https://doi.org/10.1088/1742-2132/5/3/006>
- Ghasemi, H., Zare, M., Fukushima, Y., & Koketsu, K. (2009). An empirical spectral ground-motion model for Iran. *Journal of Seismology*, 13, 499–515. <https://doi.org/10.1007/s10950-008-9143-x>
- Gülerce, Z., & Vakilinezhad, M. (2015). Effect of seismic source model parameters on the probabilistic seismic-hazard assessment results: A case study for the North Anatolian Fault zone. *Bulletin of the Seismological Society of America*, 105, 2808–2822. <https://doi.org/10.1785/0120150101>
- Hainzl, S., Scherbaum, F., & Beauval, C. (2006). Estimating background activity based on interevent-time distribution. *Bulletin of the Seismological Society of America*, 96, 313–320. <https://doi.org/10.1785/0120050053>
- Hamzehloo, H., & Mahood, M. (2012). Ground-motion attenuation relationship for East Central Iran. *Bulletin of the Seismological Society of America*, 102, 2677–2684. <https://doi.org/10.1785/0120110249>
- Hessami, K., & Jamali, F. (2006). Explanatory notes to the map of major active faults of Iran. *JSEE (iran)*, 8, 1–11.
- Idriss, I. M. (1985). Vol. 4. Technical papers: Session 6, Evaluating seismic risk in engineering practice; Session 7, \*Stability of natural deposits during earthquakes; Session 8, \*Comparison of prediction and performance of earth structures; Session 9, \*Geological aspects. A.A.Balkema, Rotterdam; Boston.
- Jackson, J. A., & Mckenzie, D. (1984). Active tectonics of the Alpine-Himalayan Belt between western Turkey and Pakistan. *Geophysical Journal of the Royal Astronomical Society*, 77, 185–264.
- Kamali, Z., Nazari, H., Rashidi, A., Heyhat, M. R., Khatib, M. M., & Derakhshani, R. (2023). Seismotectonics, geomorphology and paleoseismology of the Doroud Fault, a source of seismic hazard in Zagros. *Applied Sciences*, 13, 3747. <https://doi.org/10.3390/app1306374>
- Karimiparidari, S., Zaré, M., Memarian, H., & Kijko, A. (2013). Iranian earthquakes, a uniform catalog with moment magnitudes. *Journal of Seismology*, 17, 897–911. <https://doi.org/10.1007/s10950-013-9360-9>
- Kijko, A., Smit, A., & Sellevoll, M. A. (2016). Estimation of earthquake hazard parameters from incomplete data files. Part III. incorporation of uncertainty of earthquake-occurrence model. *Bulletin of the Seismological Society of America*, 106, 1210–1222. <https://doi.org/10.1785/0120150252>
- Maggi, A., Priestley, K., Jackson, J. A. (2002). Focal depths of moderate and large size earthquakes in Iran. *J Seismol Earthq Eng*, 4, 1–10
- Mahsuli, M., Rahimi, H., & Bakhshi, A. (2019). Probabilistic seismic hazard analysis of Iran using reliability methods. *Bulletin of Earthquake Engineering*, 17, 1117–1143. <https://doi.org/10.1007/s10518-018-0498-2>
- Maiti, S. K., & Kamai, R. (2020). Interaction between fault and off-fault seismic sources in hazard analysis—A case study from Israel. *Engineering Geology*, 274, 105723. <https://doi.org/10.1016/j.enggeo.2020.105723>
- McCall, G. J. H. (1997). The geotectonic history of the Makran and adjacent areas of southernIran. *Journal of Asian Earth Sciences*, 15(6), 517–531.
- McCall, G. J. H. (1997b). The geotectonic history of the Makran and adjacent areas of southern Iran. *Journal of Asian Earth Sciences*, 15(6), 517–531.
- McCall, G. J. H., & Kidd, R. G. W. (1982). The Makran, southeastern Iran: the anatomy of a convergent plate margin active from Cretaceous to present. In J. K. Leggett (Ed.), *Trench-forearc geology: Sedimentation and tectonics on modern and ancient active plate margins* (Vol. 10, pp. 387–397). Geological Society of London Special Publication. Blackwell Scientific.
- Mehrabi, A., Pirasteh, S., Rashidi, A., Pourkhosravani, M., Derakhshani, R., Liu, G., et al. (2021). Incorporating persistent scatterer interferometry and radon anomaly to understand the anar fault mechanism and observing new evidence of intensified activity. *Remote Sensing (basel)*, 13, 2072. <https://doi.org/10.3390/rs1312072>
- Merz, H. A., & Cornell, C. A. (1974). Seismic risk analysis based on a quadratic magnitude-frequency law. *International Journal of Rock Mechanics and Mining Sciences & Geomechanics Abstracts*, 11, 127. [https://doi.org/10.1016/0148-9062\(74\)90731-1](https://doi.org/10.1016/0148-9062(74)90731-1)
- Mirzaei, N., Gao, M. T., Chen, Y. T., & Wang, J. (1997). A uniform catalog of earthquakes for seismic hazard assessment in Iran. *Acta Seismologica Sinica Edition*, 10, 713–726. <https://doi.org/10.1007/s11589-997-0003-5>
- Mohammadi, H., & Bayrak, Y. (2016). An evaluation of earthquake hazard parameters in the Iranian Plateau based on the Gumbel III distribution. *Journal of Seismology*, 20, 615–628. <https://doi.org/10.1007/s10950-015-9547-3>



- Moinfar, A. A., Naderzadeh, A., Nabavi, M. H. (2012). New Iranian seismic hazard zoning map for new edition of seismic code and its comparison with neighbor countries. In: 15 WCEE, Lisboa 2012, p. 10.
- Mousavi-Bafrouei, S. H., Mirzaei, N., & Shabani, E. (2014). A declustered earthquake catalog for the Iranian plateau. *Annales Geophysicae*, 57, 653. <https://doi.org/10.4401/ag-6395>
- Nemati, M., & Derakhshani, R. (2021). Short-term seismicity patterns along the most active faults in Iran. *Journal of Iberian Geology*, 47, 441–459. <https://doi.org/10.1007/s41513-020-00133-0>
- Nemati, M., & Gheitanchi, M. (2011). Analysis of 2005 Dahuieh (Zarand) aftershocks sequence in Kerman province. *Journal of Earth and Space Physics (institute of Geophysics the University of Tehran)*, 37(1), 1–9.
- Nemati, M., Hajati, F. J., Rashidi, A., & Hassanzadeh, R. (2020). Seismology of the 2017 Hojedk earthquakes (MN 6.0–6.1) Kerman province, SE Iran. *Tectonophysics*, 780, 228398. <https://doi.org/10.1016/j.tecto.2020.228398>
- Nemati, M., & Tatar, M. (2015). Relations between source parameters for large Persian earthquakes. *Annals of Geophysics*, 58(5), S0543.
- Nutli, O. W. (1973). Seismic wave attenuation and magnitude relations for eastern North America. *Journal of Geophysical Research*, 78, 876–885. <https://doi.org/10.1029/jb078i005p00876>
- Ordaz, M., & Arroyo, D. (2016). On uncertainties in probabilistic seismic hazard analysis. *Earthquake Spectra*, 32, 1405–1418. <https://doi.org/10.1193/052015EQS075M>
- Rashidi, A., Abbassi, M.-R., Nilfouroushan, F., Shafiei, S., Derakhshani, R., & Nemati, M. (2020). Morphotectonic and earthquake data analysis of interactional faults in Sabzevaran Area SE Iran. *Journal of Structuring and Geology*, 139, 104147.
- Rashidi, A., & Derakhshani, R. (2022). Strain and moment rates from GPS and seismological data in Northern Iran: Implications for an evaluation of stress trajectories and probabilistic fault rupture hazard. *Remote Sensing (basel)*, 14, 2219. <https://doi.org/10.3390/rs14092219>
- Rashidi, A., Khatib, M. M., Nilfouroushan, F., Derakhshani, R., Mousavi, S. M., Kiyani, H., & Jamour, Y. (2019). Strain rate and stress fields in the West and South Lut block, Iran: Insights from the inversion of focal mechanism and geodetic data. *Tectonophysics*, 766, 94–114.
- Rashidi, A., Kianimehr, H., Shafieibafti, S., Mehrabi, A., & Derakhshani, R. (2021). Active faults in the west of the Lut block (Central Iran). *Geophysical Research*, 22, 70–84. <https://doi.org/10.21455/gr2021.3-5>
- Rashidi, A., Kianimehr, H., Yamini-Fard, F., Tatar, M., & Zafarani, H. (2022). Present stress map and deformation distribution in the NE Lut block, Eastern Iran: Insights from seismic and geodetic strain and moment rates. *Pure and Applied Geophysics*, 179, 1887–1917. <https://doi.org/10.1007/s00024-022-03015-x>
- Rashidi, A., Nemati, M., Shafieibafti, S. H., Pourbeyranvand, S. H., Derakhshani, R., & Braitenberg, C. (2023a). Structure and kinematics of active faulting in the Northern Domain of Western and Central Alborz, Iran and interpretation in terms of tectonic evolution of the Region. *Journal of Asian Earth Sciences*. <https://doi.org/10.1016/j.jseae.2023.105760>
- Rashidi, A., Shafieibafti, S., Nemati, M., Ezati, M., Gholami, E., Mousavi, S. M., & Derakhshani, R. (2023b). Flexural-slip folding in buckling phases of orogenic belts: Insight into the tectonic evolution of fault splays in the East Iran orogen. *Frontiers in Earth Science*, 11, 1169667. <https://doi.org/10.3389/feart.2023.1169667>
- Reasenber, P. (1985). Second-order moment of central California seismicity, 1969–1982. *Journal of Geophysical Research: Solid Earth*, 90, 5479–5495. <https://doi.org/10.1029/jb090ib07p05479>
- Regard, V., Bellier, O., Braucher, R., Gasse, F., Bourles, D., Mercier, J., Thomas, J.-C., Abbassi, M. R., Shabanian, E., & Soleymani, S. (2006). 10 Be dating of alluvial de-posits from Southeastern Iran (the Hormoz Strait area). *Palaeogeography, Palaeoclimatology, Palaeoecology*, 242(1), 36–53.
- Saafizaadeh, M., & Bagheripour, M. H. (2019). Evaluation of peak ground acceleration for the city of Kerman through seismic hazard analysis. *Scientia Iranica*, 26, 257–272. <https://doi.org/10.24200/sci.2017.4236>
- Saffari, H., Kuwata, Y., Takada, S., & Mahdavian, A. (2012). Updated PGA, PGV, and spectral acceleration attenuation relations for Iran. *Earthquake Spectra*, 28, 257–276. <https://doi.org/10.1193/1.3673622>
- Salahshoor, H., Lyubushin, A., Shabani, E., & Kazemian, J. (2018). Comparison of Bayesian estimates of peak ground acceleration (Amax) with PSHA in Iran. *Journal of Seismology*, 22, 1515–1527. <https://doi.org/10.1007/s10950-018-9782-5>
- Savidge, E., Nissen, E., Nemati, M., Karasözen, E., Hollingsworth, J., Talebian, M., Bergman, E., Ghods, A., Ghorashi, M., Kosari, E., Rashidi, A., & Rashidi, A. (2019). The December 2017 Hojedk (Iran) earthquake triplet - Sequential rupture of shallow reverse faults in a strike-slip restraining bend. *Geophysical Journal International*, 217, 909–925. <https://doi.org/10.1093/gji/ggz053>
- Scherbaum, F., Bommer, J. J., Bungum, H., Cotton, F., & Abrahamson, N. A. (2005). Composite ground-motion models and logic trees: Methodology, sensitivities, and uncertainties. *Bulletin of the Seismological Society of America*, 95, 1575–1593. <https://doi.org/10.1785/0120040229>
- Scordilis, E. M. (2006). Empirical global relations converting MS and mb to moment magnitude. *Journal of Seismology*, 10, 225–236. <https://doi.org/10.1007/s10950-006-9012-4>
- Sengor, A. M. C., Altner, D., Cin, A., Ustaomer, T., & Hsu, K. J. (1988). Origin and assembly of the Tethyside orogenic collage at the expense of Gondwana land. In M. G. Audley-Charles & A. E. Hallam (Eds.), *Gondwana and Tethys* (pp. 119–181). Geological Society of London Special Publication.
- Shirzad, T., Riahi, M. A., Assumpção, M. S. (2019). Crustal structure of the Collision-subduction Zone in south of Iran Using Virtual seismometers. 9, 10851, <https://doi.org/10.1038/s41598-019-47430-y>.
- Stepp, J. C. (1973). Analysis of completeness of the earthquake sample in the Puget Sound area. In: Contributions in seismic zoning, pp. 16–28.
- Stirling, M., Goded, T., Berryman, K., & Litchfield, N. (2013). Selection of earthquake scaling relationships for seismic-hazard analysis. *Bulletin of the Seismological Society of America*, 103(6), 2993–3011.
- Sucuoğlu, H., Akkar, S. (2013). Basic earthquake engineering: From seismology to analysis and design, basic earthquake engineering: From seismology to analysis and design. <https://doi.org/10.1007/978-3-319-01026-7>.
- Taghizadeh-Farahmand, F., Afsari, N., & Sodoud, F. (2015). Crustal thickness of Iran inferred from converted waves. *Pure and Applied Geophysics*, 172, 309–331.
- Taherian, A. R., & Kalantari, A. (2019). Risk-targeted seismic design maps for Iran. *Journal of Seismology*, 23, 1299–1311. <https://doi.org/10.1007/s10950-019-09867-6>
- Takin, M. (1972). Iranian geology and continental drift in the Middle East. *Nature*, 235(5334), 147–150.
- Talebi, M., Zare, M., Peresan, A., & Ansari, A. (2017). Long-term probabilistic forecast for  $M \geq 5.0$  earthquakes in Iran. *Pure and Applied Geophysics*, 174, 1561–1580. <https://doi.org/10.1007/s00024-017-1516-z>
- Talebani, M., Biggs, J., Bolourchi, M., Copley, A., Gassemi, A., Ghorashi, M., Hollingsworth, J., Jackson, J., Nissen, E., Oveisi, B., Parsons, B., Priestley, K., & Saiidi, A. (2006a). The Dahuieh (Zarand) earthquake of 2005 February 22 in central Iran:

- Reactivation of an intramountain reverse fault. *Geophysical Journal International*, 164, 137–148.
- Talebian, M., Biggs, J., Bolourchi, M., Copley, A., Ghassemi, A., Ghorashi, M., Hollingsworth, J., Jackson, J., Nissen, E., Oveisi, B., Parsons, B., Priestley, K., & Saiidi, A. (2006b). The Dahuiyeh (Zarand) earthquake of 2005 February 22 in central Iran: Reactivation of an intramountain reverse fault. *Geophysical Journal International*, 164, 137–148. <https://doi.org/10.1111/j.1365-246X.2005.02839.x>
- Tavakoli, B., & Ghafory-Ashtiany, M. (1999). Seismic hazard assessment of Iran. *Annales Geophysicae*, 42, 1013–1021.
- Trifonov, V. G., Hessami, K., Popov, S. V., Zelenin, E. A., Trikhunkov, Y. I., Frolov, P. D., Golovina, L. A., Simakova, A. N., Rashidi, A., & Latyshev, A. V. (2022). Development of the Southern coastal area of the caspian sea during the pliocene–quaternary according to biostratigraphic and magnetostratigraphic data. *Stratigraphy and Geological Correlation*, 30(4), 273–291. <https://doi.org/10.1134/S0869593822040074>
- Walker, R. T., Bergman, E. A., Elliott, J. R., Fielding, E. J., Ghods, A. R., Ghorashi, M., Jackson, J., Nazari, H., Nemati, M., Oveisi, B., Talebian, M., & Walters, R. J. (2013a). The 2010–2011 South Rigan (Baluchestan) earthquake sequence and its implications for distributed deformation and earthquake hazard in southeast Iran. *Geophysical Journal International*, 193(1), 349–374.
- Walker, R. T., Talebian, M., Sloan, R. A., Rasheedi, A., Fattahi, M., & Bryant, C. (2010). Holocene slip-rate on the Gowk strike-slip fault and implications for the distribution of tectonic strain in eastern Iran. *Geophysical Journal International*, 181(1), 221–228.
- Walker, R., Wright, T. J., & Baker, C. (2001). The 1998 March 14 Fandoqa earthquake (Mw 6.6) in Kerman province, southeast Iran: Re-rupture of the 1981 Sirch earthquake fault, triggering of slip on adjacent thrusts and the active tectonics of the Gowk fault zone. *Journal of Geophysical*, 146, 371–398.
- Yazdani, A., & Kowsari, M. (2013a). Bayesian estimation of seismic hazards in Iran. *Scientia Iranica*, 20, 422–430. <https://doi.org/10.1016/j.scient.2012.12.032>
- Yazdani, A., & Kowsari, M. (2013b). Earthquake ground-motion prediction equations for northern Iran. *Natural Hazards*, 69, 1877–1894. <https://doi.org/10.1007/s11069-013-0778-8>
- Yazdani, A., & Kowsari, M. (2017). A probabilistic procedure for scenario-based seismic hazard maps of Greater Tehran. *Engineering Geology*, 218, 162–172. <https://doi.org/10.1016/j.enggeo.2017.01.013>
- Zafarani, H., Luzi, L., Lanzano, G., & Soghrat, M. R. (2018). Empirical equations for the prediction of PGA and pseudo spectral accelerations using Iranian strong-motion data. *Journal of Seismology*, 22, 263–285. <https://doi.org/10.1007/s10950-017-9704-y>
- Zhuang, J., Ogata, Y., & Vere-Jones, D. (2002). Stochastic declustering of space-time earthquake occurrences. *Journal of American Statistical Association*, 97, 369–380. <https://doi.org/10.1198/016214502760046925>

Springer Nature or its licensor (e.g. a society or other partner) holds exclusive rights to this article under a publishing agreement with the author(s) or other rightsholder(s); author self-archiving of the accepted manuscript version of this article is solely governed by the terms of such publishing agreement and applicable law.